JOURNAL OF CATALYSIS 153, 54–64 (1995)

Isobutane Cracking over Y-Zeolites

I. Development of a Kinetic Model

G. Yaluris,* J. E. Rekoske,* L. M. Aparicio,* R. J. Madon,†,[1] and J. A. Dumesic*,[1]

*Center for Clean Industrial and Treatment Technologies, Department of Chemical Engineering, University of Wisconsin, Madison, Wisconsin 53706; and †Engelhard Corporation, 101 Wood Avenue, Iselin, New Jersey 08830

Received July 15, 1994; revised December 19, 1994

We have developed a kinetic model for isobutane cracking over calcined and steamed Y-zeolite catalysts based on carbo-cation surface chemistry. The model utilized 21 reaction steps, including initiation, oligomerization, β-scission, olefin desorption, isomerization, and hydride ion transfer, which adequately described the formation of all major products. We estimated kinetic parameters using transition state theory, the Evans–Polanyi correlation, and gas phase thermodynamic data. In order to relate the gas phase calculations to the catalyst surface, we introduced a parameter ΔH_+, which is the heat of stabilization of a carbenium ion relative to the heat of stabilization of a proton in the zeolite framework. The model provided a good description of the experimental data for calcined and steamed catalysts with physically realistic kinetic parameters. The main difference between the two catalysts was the higher ΔH_+ for the steamed catalyst. This indicates that steaming decreased the Brønsted acid strength of the catalyst.

INTRODUCTION

The importance of fluid catalytic cracking (FCC) to the refining industry has led to a significant amount of research over the last 4 decades to develop active and selective catalysts. Recent mandates of the Clean Air Act of 1990 (1) to change the overall composition of gasoline by reducing aromatics while increasing oxygenate, necessitates the development of new FCC catalysts by understanding the reactions and processes that determine the final product distribution. Studies of catalytic cracking since the early work of Greensfelder, Emmett, and their co-workers (2, 3) have led to a significant increase in our knowledge of carbenium ion chemistry over solid acids.

One of the more important developments over the last decade has been the use of the "optimum performance envelope" approach (4) of Wojciechowski and his school to study catalytic cracking of heavy oils (5, 6) and model hydrocarbons (7–9). This approach allows one to obtain initial rates and selectivities of primary and secondary products over a continuously deactivating catalyst. Various hydrocarbon reactions that take place over solid acids are well documented with general agreement concerning the essential chemical aspects of the catalytic cycles involved in catalytic cracking. Other groups (10–15) have modeled hydrocarbon reactions to provide effective ways of predicting complex product distributions. Froment and co-workers in particular have developed fundamental kinetic models for catalytic cracking (15). They generate reaction networks by computer algorithms and calculate the rate constants of each elementary step as the product of the number of single events and the single event rate constant. This approach to kinetic modeling has an advantage over lumped models in that it utilizes single-event rate constants, independent of the feedstock, which may be obtained for each catalyst by experiments with typical key hydrocarbons. In this way one may develop kinetic models for processes that involve complex hydrocarbon feedstocks. However, to our knowledge, appropriate kinetic models have not yet been used to obtain a unified description of the rates of catalytic cracking cycles. This is necessary to describe factors controlling the dependence of rates on conversion, temperature, and catalyst acidity. In this paper, we attempt to obtain such quantitative understanding of catalytic cracking cycles via microkinetic modeling (16).

Due to the complexity of such modeling, we chose to examine the reactions of a relatively simple molecule—isobutane. Isobutane, initially used by McVicker *et al.* (17) and then by others (18–20) to investigate the initiation of carbenium ions on solid acids, is an interesting molecule since its structure allows the formation of only methane and dihydrogen via any initiation route. Products

[1] To whom correspondence should be addressed.

0021-9517/95 $6.00

larger than C_4, as well as any C_3 in excess of the amount of methane produced, must be formed from cracking an oligomerized intermediate. Our initial attempts at microkinetic modeling of isobutane cracking have been described elsewhere (16, 21). Here we present a more detailed account of the model to allow us to describe the catalytic cycles that manifest during the cracking process. This paper focuses on formulating a kinetic model using well-known concepts of carbo-cation chemistry, parameterizing the reaction steps in the model, and calibrating the model to our experimental data for isobutane cracking over commercial ultrastable Y-zeolite (USY) catalysts. In the following paper (22), we use this model to analyze the catalytic cycles that occur during isobutane cracking, address factors controlling the reaction steps, and describe the roles that these steps play in determining selectivity and activity.

EXPERIMENTAL

Catalysts

The USY-based FCC catalyst was made via the Engelhard *in situ* zeolite crystallization process (23, 24) in which Y-zeolite is crystallized on a calcined kaolin microsphere. The zeolite-containing microspheres were subjected to exchanges with ammonium nitrate and calcinations. The USY-C catalyst was prepared by further calcining the material at 840 K for 2 h, whereas USY-S was prepared by fluidizing it in 100% steam at atmospheric pressure and 1060 K for 2 h. The USY-C catalyst has properties similar to a fresh FCC catalyst before it is added to a commercial unit, whereas the steamed USY-S mimics an FCC catalyst in the unit after it has undergone some dealumination and deactivation. The catalysts contained 0.3 wt% Na_2O. Other physical properties of these catalysts are listed in Table 1. Nitrogen BET of the entire sample minus the surface area of pores larger than 2 nm diameter, obtained as a "*t*" plot, gave the microporous surface area. The latter area is mainly that of the zeolite component. Unit cell size measurements via X-ray diffraction were performed using a Si standard, and the framework Al per unit cell were obtained via the correlation given by Sohn *et al.* (25).

TABLE 1

Properties of Catalysts

Catalyst	USY-C	USY-S
Zeolite surface area (m^2/g)	274	221
Total surface area (m^2/g)	418	349
Zeolite content (%)	38	31
Unit cell size (Å)	24.43	24.30
Al_F[a]	20.56	6.64
Si/Al	8.3	27.9
Brønsted sites (μmol/g)[b]	532	52
Lewis sites (μmol/g)[b]	304	81

[a] Number of framework Al atoms per unit cell.

[b] Measured by infrared spectroscopy of adsorbed pyridine as described in text.

Procedures

We carried out the kinetic experiments in a standard flow unit containing Brooks flow controllers and a three-zone furnace controlled by Eurotherm temperature controllers. We used a Pyrex flow reactor, 1.27 cm in diameter and 56 cm in length. The top of the reactor was filled with quartz rings and served as a preheating zone, while the catalyst was supported in the lower third of the reactor with quartz wool. A mixture of 25 mol% isobutane in He (Liquid Carbonic, 99.999% purity) was used in all experiments, and total flow rates were adjusted to achieve the desired conversion. Isobutane obtained from Matheson was better than 99.5% pure with oxygen concentration in the low ppm level; the contaminants, propane and *n*-butane, were corrected for in the experimental data. Reaction products were collected in a Valco multiport valve in separate sampling loops (20 cm^3). The first sample was collected after 2–4 min reaction time, and typically four samples were collected at time intervals of 1–2 min. The data reported here are usually from the first loop. No selectivity changes were observed from one loop to the other, while conversions changed only slightly due to catalyst deactivation. The catalyst was purged between runs with flowing He (200 cm^3/min) for about 2 h and then regenerated in flowing air (200 cm^3/min) at 773 K for 8 h. Kinetic data were collected for catalyst USY-C at temperatures between 733 and 773 K, and at 773 K for USY-S.

We analyzed hydrogen and hydrocarbon products simultaneously with an automated multivalved Hewlett Packard 5890A gas chromatograph containing two columns and two detectors. A 150-m capillary column (Supelco Petrocol DH150) provided complete separation of the hydrocarbon products, and amounts as low as 0.0005 mol% were easily detected with a flame ionization detector. A Porapak P column was used to separate hydrogen from the hydrocarbons and this hydrogen was detected by a thermal conductivity detector.

We used infrared spectroscopy of adsorbed pyridine to measure Brønsted and Lewis acidity. The experiments were carried out in a diffuse reflectance mode using a Spectra Tech controlled-environment chamber in a Perkin–Elmer 1750 spectrometer. Measurements were quantified using extinction coefficients that were specifically obtained for this instrument using a series of aluminosilicate samples. Experimental details are given in Ref. (26) and the results in Table 1.

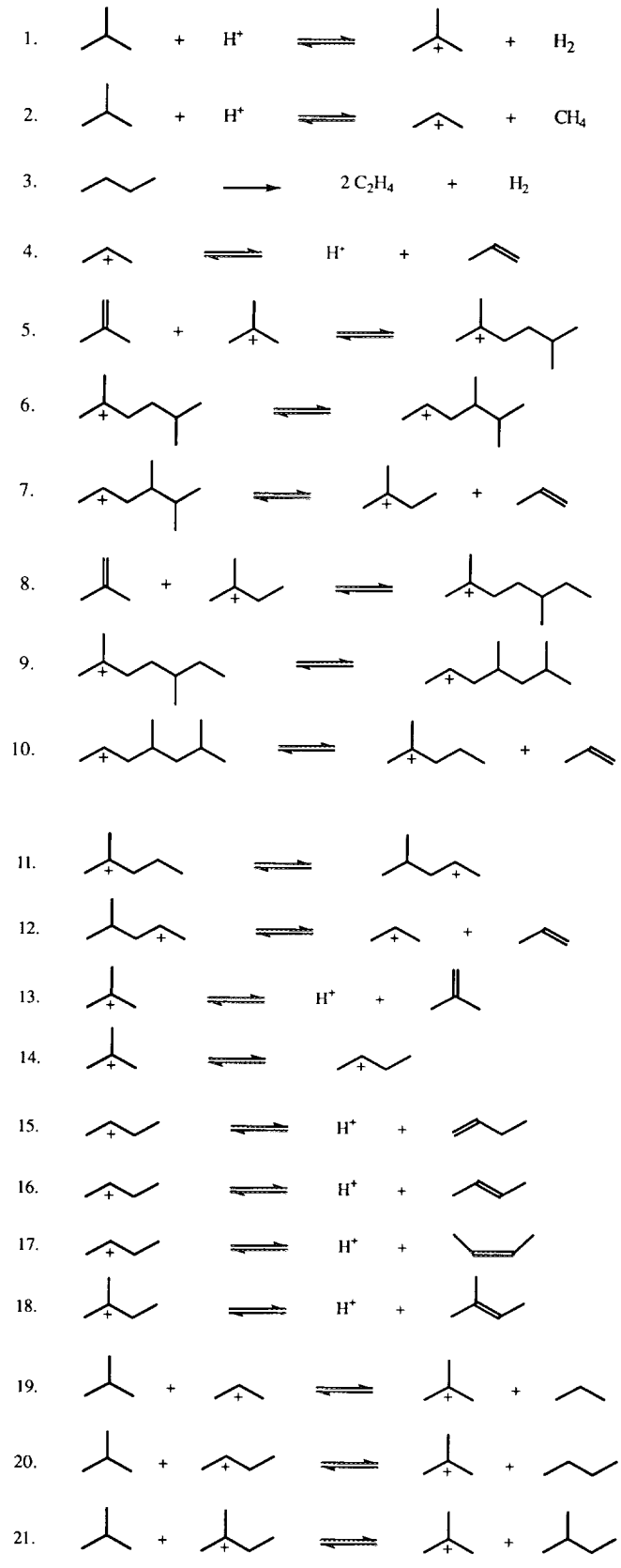

FIG. 1. Reaction scheme for isobutane cracking.

DEVELOPMENT OF A KINETIC MODEL

General Approach

The primary difficulty in developing a kinetic model based on reasonable surface chemistry is that such models often contain large numbers of surface reaction steps for which kinetic rate constants must be estimated (12–16). Therefore, the formulation of the reaction mechanism involves a compromise between the desire to write all steps as elementary processes and the problem of estimating rate constants for all of these steps.

Our model (21) for isobutane cracking contains 21 steps (Fig. 1) that describe the formation of 12 main products. A kinetic model containing 21 reversible steps requires estimating 42 preexponential factors and an equal number of activation energies. The independent products of the reaction lead to 12 equilibrium constraints for the preexponential factors and an equal number for the activation energies. Since 60 kinetic parameters are still too many for meaningful kinetic analysis with the available experimental data, parameterization of the kinetic model is necessary.

The object of parameter estimation is to develop a procedure applicable systematically to various hydrocarbon species in order to derive rate constants consistent with reaction thermodynamics. Successful calibration of a general procedure for rate constant estimation may allow us to estimate rate constants for reactions of other hydrocarbons on acid zeolites. Our approach is to first estimate standard entropy and enthalpy changes of reaction for all steps, assuming that reactions take place in the gas phase, and then to adjust these values for surface reactions by making reasonable assumptions about the mobility and chemical bonding of various species on the acid sites.

Whereas the initial formulation of a kinetic model requires more detailed information than is generally available, only a fraction of these rate constants are kinetically significant in the final kinetic model. The model is used primarily to predict rates of reactions; the rate constants and surface coverages used for such predictions cannot necessarily be determined separately. For example, the proper rate may be obtained with different surface coverages provided that rate constants are adjusted accordingly. Therefore, surface coverages predicted by the model may only be used for comparative purposes. Similarly, the model may work well over a specific temperature range with different values of preexponential factors, provided one compensates by adjusting the activation energies.

Model Formulation

It is not intended via microkinetic analysis to prove a mechanism but rather to see if a sequence of reaction steps

chosen to describe the overall chemistry is reasonable and allows us to explain observed activity and selectivity relationships. We have used well-known concepts in carbo-cation chemistry (27–29) to formulate 21 reaction steps (Fig. 1), the same as those used earlier (16, 21), to account for 12 major products: hydrogen, methane, ethylene, propylene, propane, *n*-butane, isobutylene, 1-butene, *trans*-2-butene, *cis*-2-butene, isopentane, and 2-methyl-2-butene. Though the role of Brønsted acid sites in acid catalyzed cracking has been well accepted since the early work of Ward (30) and others (31–33), the importance of Lewis acidity is unclear. Suggestions have been made that Lewis acid sites may act in conjunction with Brønsted acid sites (34, 35) or increase the strength of Brønsted acid sites (34–38). These are issues that can be addressed by our model when they are better understood. For the present, we assume that only Brønsted acid sites are active for isobutane cracking.

Initiation of carbenium ions from isobutane may take place via protolysis (18, 39), via H^- abstraction by a Lewis acid site (40), or via the protonation of alkenes formed by the decomposition of surface-assisted isobutyl radical cations generated on electron acceptor sites (17, 41). In any case, initiation processes involving pentacoordinated carbonium ions and radical cation mechanisms are kinetically equivalent and cannot be distinguished by kinetic analysis, since both processes are first-order with respect to hydrocarbon pressure. Therefore, the choice of an initiation process for the kinetic model is arbitrary. For simplicity and to ensure that the number of parameters is not increased, we chose protolysis as the initiation mechanism for isobutyl and propyl carbenium ions (steps 1 and 2, Fig. 1).

Once carbenium ions form, they can participate in a variety of reactions. *n*-Butane and butenes are produced from isobutane by the isomerization of an isobutyl cation to form an *n*-butyl cation (step 14) which can abstract a hydride ion from isobutane to give *n*-butane and isobutyl cations (step 20). This chain is terminated when the isobutyl or *n*-butyl cation desorbs as an olefin (steps 13 and 15–17). The isomerization is probably a concerted event involving a primary carbenium ion leading to a protonated methyl cyclopropyl transition state (42). Hilaireau and co-workers (43) proposed that the formation of *n*-butyl cations involves C_8 species formed via oligomerization reactions. However, this pathway was not utilized in this work due to insufficient supporting experimental data (44, 45).

The hydride ion transfer step is written as an Eley–Rideal step where a surface carbenium ion apparently reacts with a gas phase paraffin. It is probable, however, that the paraffin adsorbs weakly as a precursor state adjacent to the surface carbenium ion prior to reaction (46). Our choice of an apparent Eley–Rideal reaction step to describe hydride ion transfer is kinetically equivalent to the reaction of an adsorbed paraffin provided that the sites on which the paraffin adsorbs do not become saturated. This assumption seems to be justified by the model which indicates that under any conditions most of the sites are available.

Isopentane is formed via a combination of oligomerization, isomerization, and β-scission steps (9, 17, 44). Alkylation of isobutyl cations with isobutylene results in a C_8^+ intermediate which undergoes β-scission to give propylene and isopentyl cations (steps 5–7). The latter undergo hydride ion transfer with isobutane to give isopentane (step 21) or desorb as 2-methyl-2-butene (step 18). Hydride ion transfer from an isobutane molecule to a surface propyl cation results in propane formation (step 19). Our experimental data show that the yield of C_3 species is greater than the sum of the yields of CH_4 and C_5 species. Hence, the formation of the propyl cation (step 2) and its subsequent desorption (step 4) as well as oligomerization and β-scission (steps 5–7) do not account for all the C_3 species produced. Therefore, additional routes for the production of C_3 species are required. The pathway we chose (21) consists of alkylating the isopentyl cation by isobutylene to form C_9^+ species which undergo β-scission and isomerization reactions to form propylene and propyl cations (steps 8–12). While the oligomerization/β-scission processes that we suggest may not represent all possible reactions, they appear to be sufficient to account for all the major products. We chose to depict the oligomerization reaction as a concerted process in which a relatively unstable primary carbenium ion complex reacts with an unsaturated carbon following Markownikoff addition rules. Energetically, the difference between the unstable intermediate and the final transition state is probably negligible. Oligomerizations may also be written as Markownikoff additions of a tertiary carbenium ion to an unsaturated carbon that result in species containing a quartenary carbon followed by a series of skeletal isomerizations (47). Kinetically, the choice is not important.

Finally, it is difficult to account for ethylene formation via a carbenium ion mechanism, because this requires surface stabilization of a relatively unstable primary carbenium ion. Other routes via free radical processes (17, 48, 49) are possible but have not been established. Due to this uncertainty, we have written ethylene formation as an irreversible step involving *n*-butane (step 3).

Preexponential Factors

We used the transition state theory to estimate preexponential factors for the kinetic model (50)

$$k = \frac{k_B T}{h} e^{\Delta S^{\neq}/R} e^{-\Delta H^{\neq}/RT}, \qquad [1]$$

where k_B is the Boltzmann constant, h is the Planck constant, $\Delta S^{\neq}$ is the standard entropy change, and $\Delta H^{\neq}$ is the enthalpy change from reactants to the transition state. If we use an Arrhenius expression for the rate constant

$$k = Ae^{-E_a/RT}, \quad [2]$$

then it is sufficient within the accuracy of the present study to equate the activation energy, E_a, to $\Delta H^{\neq}$ and the preexponential factor, A, becomes

$$A = \frac{k_B T}{h} e^{\Delta S^{\neq}/R}. \quad [3]$$

Equation [3] requires estimates for the absolute entropies of all species participating in the various reaction steps, including the transition states. We obtained the entropies of gaseous species from tables of thermodynamic properties (51, 52), and calculated or estimated the entropies of carbenium ions in the gas phase from data on gas phase basicity and proton affinities reported by Aue and Bowers (53). For example, we assumed an average value of −27.9 cal mol^{-1} K^{-1} for the standard entropy change of the protonation reaction at 298 K

$$\text{Olefin} + H^+ \rightarrow \text{Carbenium ion}. \quad [4]$$

The absolute entropy of gaseous H^+ is equal to 26.01 cal mol^{-1} K^{-1} at 298 K and 1 atm (54).

For estimating the entropies of transition states, we assumed: (a) for protolysis steps the transition state to be similar to the reacting paraffin; (b) for carbenium ion isomerization steps the transition state to be similar to an intermediate form of the two carbenium ions; (c) for β-scission and olefin adsorption steps the transition state to be similar to the corresponding carbenium ion; and (d) for hydride ion transfer steps the transition state to be similar to the paraffin corresponding to a combination of the reactants in the step.

We corrected absolute entropies at 298 K to 773 K using tabulated relations for heat capacities (55). Heat capacities for carbenium ions were assumed to be equal to those of the corresponding olefins. Heat capacities for transition states were assumed to be equal to those for the corresponding paraffins or olefins as described above.

The translational contributions to the absolute entropies of all species were calculated using the equation (56)

$$S_{trans} = k_B N \left\{ \ln \left[\frac{(2\pi m k_B T)^{3/2}}{h^3} \right] + \ln \left(\frac{V}{N} \right) + \frac{5}{2} \right\}, \quad [5]$$

where N is Avogadro's number, m is the molecular mass, and V is the molar volume at temperature T.

The entropies of surface species and transition states may be expressed in terms of standard entropy changes of adsorption. While experimental measurements of these entropy changes have not yet been made for species used in our model, we adopted a reasonable strategy for making such estimates. We made assumptions that gave low coverage of the Brønsted acid sites by carbenium ions under reaction conditions for isobutane cracking, since carbenium ions have not been directly observed on working cracking catalysts. According to this approach, all of the vibrational and rotational entropy is maintained during adsorption. For C_n species with $n \leq 6$, translational entropy corresponding to 1/2 of one degree of freedom was assumed to be maintained after adsorption. For C_n species with $n \geq 7$, only 1/3 of one degree of freedom of translational entropy was assumed to be maintained after adsorption. For transition states of reactions involving gas phase and surface species, an additional degree of freedom of translational entropy was maintained upon adsorption compared to a similar surface species. Since hydride ion transfer reactions proceed through bulky transition states of poorly understood structure, we assumed that the corresponding transition state maintains one degree of translational freedom of the corresponding gas phase species. These assumptions agree with measurements of the entropy of adsorption of ammonia on H-mordenite and

TABLE 2

Reaction Entropy Changes and Preexponential Factors Estimated at 773 K

	ΔS (cal mol^{-1} K^{-1})	$\Delta S^{\neq}$ (Forward) (cal mol^{-1} K^{-1})	Preexponential factors (s^{-1} or s^{-1} $Torr^{-1}$)	
			Forward	Reverse
Step 1	−4.84	−21.42	4.42×10^5	5.05×10^6
Step 2	−0.66	−21.42	4.42×10^5	6.17×10^5
Step 3	−21.42		2.78×10^{12}	0
Step 4	37.13	13.98	1.83×10^{16}	1.85×10^5
Step 5	−38.38	−23.44	1.60×10^5	2.97×10^{16}
Step 6	−0.33	−0.16	1.48×10^{13}	1.75×10^{13}
Step 7	43.47	14.94	2.97×10^{16}	1.24×10^4
Step 8	−38.40	−23.34	1.68×10^5	3.15×10^{16}
Step 9	−1.51	−0.76	1.10×10^{13}	2.36×10^{13}
Step 10	41.88	15.06	3.15×10^{16}	2.92×10^4
Step 11	−2.19	−1.10	9.28×10^{12}	2.80×10^{13}
Step 12	38.26	14.66	2.57×10^{16}	1.47×10^5
Step 13	38.50	14.26	2.11×10^{16}	1.07×10^5
Step 14	1.91	0.95	2.60×10^{13}	9.96×10^{12}
Step 15	39.09	14.26	2.11×10^{16}	7.94×10^4
Step 16	36.83	14.26	2.11×10^{16}	2.48×10^5
Step 17	36.56	14.26	2.11×10^{16}	2.84×10^5
Step 18	36.36	14.48	2.35×10^{16}	3.50×10^5
Step 19	−0.61	−24.58	8.99×10^4	1.22×10^5
Step 20	1.62	−23.76	1.36×10^5	6.01×10^4
Step 21	0.01	−25.67	5.20×10^4	5.17×10^4

H-ZSM-5 (57), where ammonia retains its rotational and vibrational entropy and loses its translational entropy upon adsorption on strong acid sites.

Table 2 summarizes values of preexponential factors calculated by Eq. [3] for forward and reverse rate constants of each reaction step. Since step 3 (ethylene production) is not an elementary step, the preexponential factor for this step was left as an adjustable parameter. The set of preexponential factors employed in this study is not unique for describing the kinetics of isobutane cracking. However, the values are consistent with the overall reaction thermodynamics and are based on reasonable estimates for the entropies of adsorbed species and transition states. Without additional experimental data, we cannot provide better estimates for these preexponential factors, and these values will not be adjusted further in our kinetic analyses.

Activation Energies

We parameterized activation energies using known thermodynamic properties of hydrocarbons and carbenium ions in the gas phase. The approach was analogous to that used for the preexponential factors. We used the Evans–Polanyi correlation to express activation energies in terms of enthalpies of reactions, ΔH (16)

$$E_\alpha = E_0 + \alpha \Delta H, \qquad [6]$$

where E_0 and α are constants for a given family of reactions. For simplicity, the value of α was set equal to 0.5 for all reactions. In cases where Eq. [6] predicted a negative value of the activation energy, the value of E_α was set equal to zero and the activation energy of the opposite step was set equal to the absolute value of the heat of reaction, ΔH.

We obtained heats of formation of gas phase species at 298 K from Refs. (51, 52), and heats of formation for some carbenium ions in the gas phase from data reported by Aue and Bowers (53). In cases where tabulated data were not available, we estimated heats of formation for carbenium ions by extrapolating data available for the reaction of tertiary carbenium ions with a hydride ion to form the corresponding paraffin

$$\text{Tertiary Carbenium Ion} + H^- \rightarrow \text{Paraffin}. \qquad [7]$$

An average value for the heat of this reaction at 298 K is −228 kcal/mol (53), and the heat of formation of H^- is 33.2 kcal/mol (54). Since the heats of formation of secondary carbenium ions are generally about 18 kcal/mol higher than those of tertiary carbenium ions, this value was used to estimate the heats of formation of the remaining secondary carbenium ions. The heats of formation of the gas phase species were corrected for the reaction temperature (773 K) as described above for the entropies.

To obtain heats of reaction, we first calculated gas phase enthalpy changes of reaction for all steps. Subsequently, in order to account for the participation of surface species, we introduced a parameter ΔH_+, the heat of stabilization of a carbenium ion relative to the heat of stabilization of a proton in the zeolite framework. We assumed for simplicity that this parameter was the same for all carbenium ions. The value of ΔH_+ is related to the Brønsted acid strength of the catalyst; the lower the value, the stronger the acid site since the difference between the heat of stabilization of a carbenium ion and a proton is smaller. The value of this parameter includes a large, catalyst-independent constant that is related to the high heats of formation of gas phase protons (367.2 kcal/mol at 298 K (54)) and gas phase carbenium ions. Only a small fraction of this value is dependent on the acidity of the catalyst. Therefore, small changes in the value of ΔH_+ are meaningful and represent significant changes in the acid strength of the catalyst.

The Evans–Polanyi correlation allows a single parameter, E_0, to be used to relate activation energies for reaction steps in a common reaction family. We grouped the reaction families as follows: olefin adsorption/desorption reactions (steps 4, 13 and 15–18), carbenium ion isomerization reactions involving tertiary and secondary ions (steps 6, 9, 11, and 14), oligomerization reactions involving rearrangements between tertiary and primary carbenium ions (steps 5 and 8), and β-scission reactions (steps 7 and 10) where isomerization of a secondary to tertiary carbenium ion occurs. We treated the β-scission reaction (step 12) separately since it involves no rearrangement of the resulting carbenium ion. We did not group the protolysis reactions (steps 1 and 2) into one reaction family because each reaction involves the breaking of a different bond (C–H and C–C bonds) and has a different transition state. Hydride ion transfer reactions (steps 19, 20, and 21) were initially classified in one reaction family, but the Evans–Polanyi constants of these steps were allowed to change slightly in the later stages of the data fitting procedure. Finally, we assigned a separate Evans–Polanyi parameter to the ethylene production reaction.

Depending on the experimental conditions, several researchers (8, 9, 17, 44) have reported that olefin adsorption steps involving Brønsted acid sites and formation of carbenium ions are equilibrated processes. In the present study, the experimental ratios of the partial pressures of isobutylene and *n*-butenes are independent of conversion, indicating that C_4 olefins are equilibrated. Furthermore, we obtained good fits of the experimental data with small values of the Evans–Polanyi constants of these reactions and isomerization steps. Therefore, we assumed the isom-

erization and olefin adsorption/desorption processes to be quasi-equilibrated, and set the Evans–Polanyi constants of reactions 4, 6, 9, 11, and 13–18 to zero.

Calibration of the Kinetic Model

Our kinetic model initially consisted of the following 11 parameters: ΔH_+, the preexponential factor of step 3, and the Evans–Polanyi parameters of steps 1, 2, 3, 5, 7, 12, 19, 20, and 21.

We used a computer software program (58) to adjust the kinetic parameters to fit the experimental partial pressures of 12 gaseous product species under 10 sets of experimental conditions (space velocity, pressure, and temperature) for catalyst USY-C. This program employs the Rosenbrock method to minimize a weighted least-square objective function. The choice for weight factors depends on the reliability of the experiment fitted and the amounts in the product stream of the species simulated. Thus the optimization procedure can be modified to take into account experimental uncertainties and to fit both major and minor products, i.e., species of both high and low partial pressures in the product stream.

We assumed the reactor to be a plug-flow reactor and neglected the pressure drop through the reactor. Experimental data were used without corrections for gas phase reactions (thermal cracking), since blank experiments gave conversions of less than 1%. During the optimization procedure, we found the Evans–Polanyi parameters for steps 7 and 12 to be kinetically insignificant, and therefore *the final optimization required only nine adjustable parameters*. Table 3 lists the values of the Evans–Polanyi parameters and activation energies for all reaction steps.

TABLE 3

Reaction Enthalpy Changes and Activation Energies for Catalyst USY-C Estimated at 773 K

	Catalyst USY-C, ΔH_+ = 164.4 kcal mol^{-1}			
	ΔH_{rxn} (kcal mol^{-1})	E_0 (kcal mol^{-1})	$E_{\alpha,for}$ (kcal mol^{-1})	$E_{\alpha,rev}$ (kcal mol^{-1})
Step 1	−7.56	42.68	38.90	46.46
Step 2	−2.43	39.31	38.09	40.52
Step 3	55.95	31.42	59.40	
Step 4	20.76	0	20.76	0
Step 5	−19.25	35.12	25.50	44.75
Step 6	18.00	0	18.00	0
Step 7	3.38	18.74	20.43	17.05
Step 8	−17.62	35.12	26.31	43.93
Step 9	18.00	0	18.00	0
Step 10	2.64	18.74	20.06	17.42
Step 11	18.34	0	18.34	0
Step 12	22.76	20	31.38	8.62
Step 13	36.84	0	36.84	0
Step 14	17.60	0	17.60	0
Step 15	23.10	0	23.10	0
Step 16	20.39	0	20.39	0
Step 17	20.79	0	20.79	0
Step 18	36.71	0	36.71	0
Step 19	−17.62	26.13	17.32	34.94
Step 20	−15.70	23.75	15.90	31.60
Step 21	1.81	28.94	29.84	28.03

TABLE 4

Reaction Enthalpy Changes and Activation Energies for Catalyst USY-S Estimated at 773 K

	Catalyst USY-S, ΔH_+ = 166.3 kcal mol^{-1}			
	ΔH_{rxn} (kcal mol^{-1})	E_0 (kcal mol^{-1})	$E_{\alpha,for}$ (kcal mol^{-1})	$E_{\alpha,rev}$ (kcal mol^{-1})
Step 1	−5.59	42.24	39.45	45.03
Step 2	−0.46	39.74	39.51	39.97
Step 3	55.95	32.49	60.46	
Step 4	18.79	0	18.79	0
Step 5	−19.25	35.06	25.44	44.69
Step 6	18.00	0	18.00	0
Step 7	3.38	18.74	20.43	17.05
Step 8	−17.62	35.06	26.25	43.87
Step 9	18.00	0	18.00	0
Step 10	2.64	18.74	20.06	17.42
Step 11	18.34	0	18.34	0
Step 12	22.76	20	31.38	8.62
Step 13	34.87	0	34.87	0
Step 14	17.60	0	17.60	0
Step 15	21.13	0	21.13	0
Step 16	18.41	0	18.41	0
Step 17	18.82	0	18.82	0
Step 18	34.74	0	34.74	0
Step 19	−17.62	26.43	17.62	35.24
Step 20	−15.70	23.58	15.73	31.43
Step 21	1.81	28.31	29.22	27.41

The kinetic parameters obtained in the analysis of isobutane cracking over USY-C were subsequently used as initial values to describe the catalytic behavior of USY-S. We allowed the Evans–Polanyi constant of step 3 and ΔH_+ to change for USY-S, while keeping the remaining parameters for USY-C unchanged. The results of the fitting procedure captured the essential changes in catalytic properties between these two materials. Subsequently, all eight parameters were allowed to adjust (the preexponential factor of step 3 was kept constant) to achieve a better quantitative description of the trends in the experimental data for USY-S. Except for a large change of 1.97 kcal/mol in ΔH_+, which reflects the difference in the catalysts, other parameters were only marginally modified. Table 4 lists the results for USY-S. Comparison of Tables 3 and 4 shows that differences in the heats of reaction to be due to the 1.97 kcal/mol difference in ΔH_+. For steps with nonzero values of E_0, steps 5, 7, 8, 10, 12, 19, 20, and 21, where the effect of ΔH_+ cancels out, the E_α values for the two catalysts are extremely close.

TABLE 5

Experimental Data and Model Predictions for Isobutane Cracking over USY-C Catalyst at 773 K and at Different Space Velocities (All Values are Mol % of the Reactor Effluent Stream)

S_v^{-1} (g h/mol)	5.16		6.62		8.10		10.76		13.11		16.16	
Pressure (kPa)	151.7		139.7		137.3		130.1		127.7		122.8	
Conversion (%)	11.2		16.5		19.7		27.7		32.3		40.5	
	Exp	Model	Exp	Model	Exp	Model	Exp	Model	Exp	Model	Exp	Model
Hydrogen	0.278	0.290	0.428	0.356	0.501	0.431	0.622	0.556	0.715	0.730	0.777	0.829
Methane	0.376	0.417	0.480	0.492	0.539	0.560	0.666	0.662	0.814	0.779	0.873	0.825
Ethylene	0.077	0.087	0.138	0.132	0.187	0.200	0.336	0.331	0.505	0.541	0.635	0.683
Propylene	0.298	0.301	0.423	0.393	0.496	0.500	0.687	0.687	0.842	0.934	0.893	1.096
Propane	0.619	0.692	0.976	0.957	1.204	1.288	1.896	1.919	2.718	2.710	3.383	3.371
n-Butane	0.855	0.927	1.174	1.172	1.352	1.417	1.771	1.827	2.195	2.192	2.426	2.508
C_4 olefins	0.377	0.404	0.447	0.464	0.479	0.516	0.530	0.600	0.598	0.699	0.573	0.753
2-Methyl-2-butene	0.011	0.021	0.017	0.027	0.023	0.033	0.032	0.043	0.044	0.054	0.047	0.062
Isopentane	0.304	0.304	0.463	0.424	0.556	0.561	0.753	0.791	0.892	1.017	0.947	1.185

RESULTS

The experimental data and the corresponding results given by the kinetic model (Tables 5–7) show good agreement for USY-C and USY-S. The model properly predicts a complex product distribution using a limited number of kinetic parameters based on surface chemistry typically associated with acid catalysts.

Tables 5 and 6 show that the model for USY-C accurately predicted the trends observed experimentally with conversion and temperature for hydrogen, methane, ethylene, propane, and *n*-butane. Figures 2 and 3 show the changes with conversion and temperature in the fractions of C_3, C_4, and C_5 species in the C_3–C_5 product stream. Both the experimental data and our model indicate that the fraction of C_3 species increases continuously for conversions above 10%, whereas, the fraction of C_4 species decreases with increasing conversion. The fraction of C_5 species initially increases and then may decrease slightly at high conversions. Increasing temperature has a similar effect as increasing conversion. Some discrepancies between the model predictions and the experimental data are apparent for propylene, C_4 olefins, isopentane, and 2-methyl-2-butene. These discrepancies are limited to high conversions, with the exception of 2-methyl-2-butene which is generally overestimated. However, the trend predicted by the model for variations with temperature for this species is good.

Figures 4 and 5 compare site time yields of paraffins (methane and higher) and olefins (ethylene and higher) observed experimentally and predicted by the model. Site time yield of a product is defined as the rate of formation

TABLE 6

Experimental Data and Model Predictions for Isobutane Cracking over USY-C Catalyst at Isobutane Space Velocity of 0.062 mol g^{-1} h^{-1} and at Different Temperatures (All Values are Mol % of the Reactor Effluent Stream)

Temperature (K)	733		743		753		762		773	
Pressure (kPa)	125.2		125.2		127.7		125.7		122.8	
Conversion (%)	12.4		17.6		23.5		29.9		40.5	
	Exp	Model	Exp	Model	Exp	Model	Exp	Model	Exp	Model
Hydrogen	0.118	0.159	0.275	0.248	0.374	0.390	0.542	0.546	0.777	0.829
Methane	0.254	0.242	0.368	0.347	0.510	0.484	0.640	0.618	0.873	0.825
Ethylene	0.054	0.040	0.118	0.095	0.227	0.216	0.361	0.367	0.635	0.683
Propylene	0.186	0.174	0.309	0.307	0.477	0.520	0.642	0.736	0.893	1.096
Propane	0.729	0.745	1.176	1.212	1.782	1.922	2.305	2.490	3.383	3.371
n-Butane	1.213	1.312	1.575	1.684	1.911	2.106	2.151	2.295	2.426	2.508
C_4 olefins	0.258	0.259	0.346	0.355	0.479	0.424	0.500	0.588	0.573	0.753
2-Methyl-2-butene	0.009	0.013	0.016	0.022	0.027	0.034	0.036	0.045	0.047	0.062
Isopentane	0.443	0.402	0.631	0.605	0.804	0.857	0.868	1.005	0.947	1.185

TABLE 7

Experimental Data and Model Predictions for Isobutane Cracking over USY-S Catalyst at 773 K and at Different Space Velocities (All Values are Mol % of the Reactor Effluent Stream)

S_v^{-1} (g h/mol)	114.9		135.1		232.6	
Pressure (kPa)	137.3		137.3		127.7	
Conversion (%)	10.0		12.9		21.1	
	Exp	Model	Exp	Model	Exp	Model
Hydrogen	0.485	0.440	0.475	0.485	0.835	0.837
Methane	0.381	0.393	0.418	0.426	0.695	0.663
Ethylene	0.073	0.063	0.100	0.084	0.280	0.295
Propylene	0.409	0.370	0.451	0.427	0.762	0.849
Propane	0.482	0.417	0.582	0.505	1.494	1.376
n-Butane	0.735	0.677	0.795	0.765	1.490	1.542
C_4 olefins	0.493	0.447	0.483	0.470	0.608	0.658
2-Methyl-2-butene	0.013	0.019	0.017	0.021	0.036	0.040
Isopentane	0.272	0.235	0.332	0.289	0.682	0.745

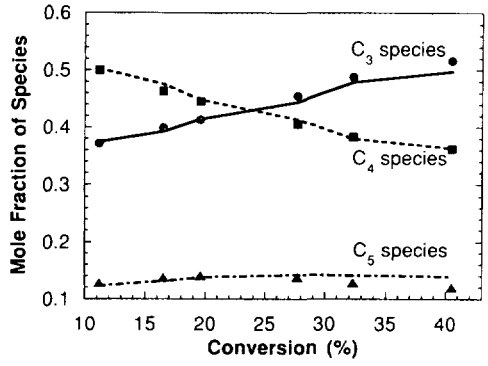

FIG. 2. Simulated and experimental distributions of C_3, C_4, and C_5 species for isobutane cracking over USY-C at 773 K and various conversions. Values in mole fractions of the total amount of C_3, C_4, and C_5 species in the gas phase. Points represent experimental data.

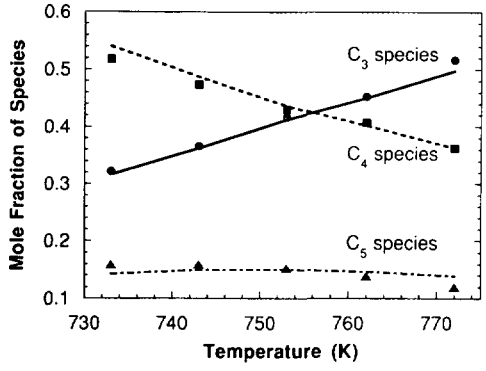

FIG. 3. Simulated and experimental distributions of C_3, C_4, and C_5 species for isobutane cracking over USY-C at isobutane space velocity 0.062 mol g^{-1} h^{-1} and various temperatures. Values in mole fractions of the total amount of C_3, C_4, and C_5 species in the gas phase. Points represent experimental data.

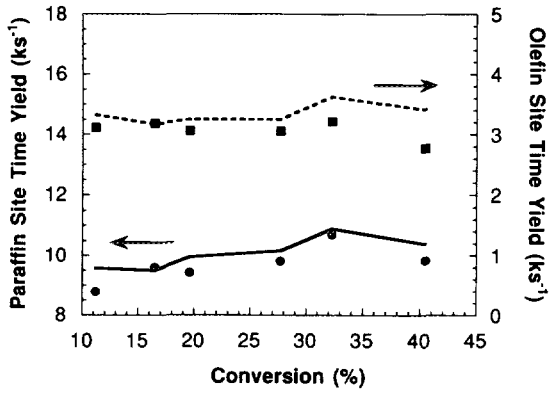

FIG. 4. Simulated and experimental paraffin and olefin site time yields for catalyst USY-C at 773 K and various conversions. Points represent experimental data.

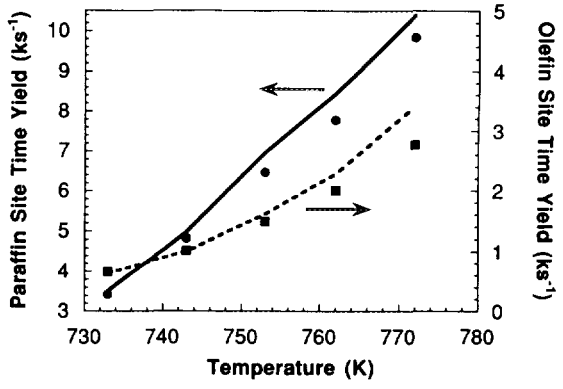

FIG. 5. Simulated and experimental paraffin and olefin site time yields for catalyst USY-C at isobutane space velocity 0.062 mol g^{-1} h^{-1} and various temperatures. Points represent experimental data.

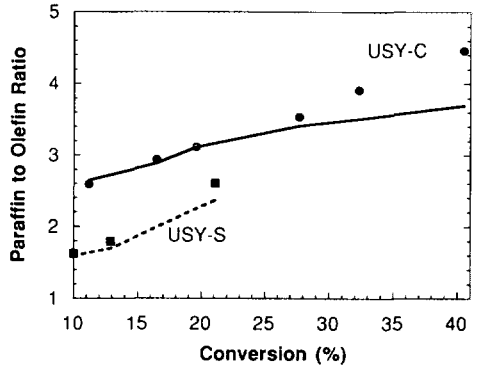

FIG. 6. Simulated and experimental paraffin to olefin ratios for isobutane cracking over catalysts USY-C and USY-S at 773 K and various conversions. Paraffins and olefins with three or more carbon atoms are counted. Points represent experimental data.

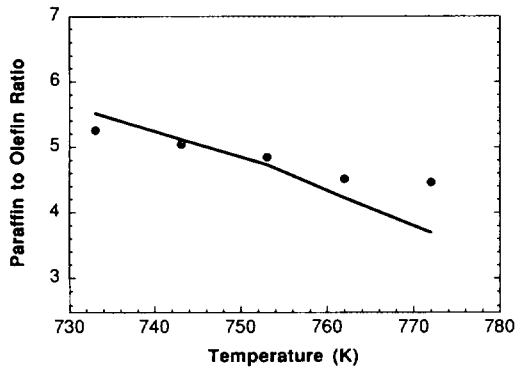

FIG. 7. Simulated and experimental paraffin to olefin ratios for isobutane cracking over catalyst USY-C at isobutane space velocity 0.062 mol g^{-1} h^{-1} and various temperatures. Paraffins and olefins with three or more carbon atoms are counted. Points represent experimental data.

of that product in terms of molecules produced in the reactor per catalytic site and time unit. The model satisfactorily predicts rates of formation for both paraffins and olefins. Discrepancies found primarily at high conversions may be due to processes that were not taken into account. For example, C_5 species are more reactive than isobutane, and subsequent reactions involving these species should be included at higher isobutane conversions. Furthermore, the formation of coke from olefins is not included in our model.

Results shown in Figs. 6 and 7 for catalysts USY-C and USY-S indicate that our model correctly predicts the change of the paraffin to olefin ratio with respect to conversion at a constant temperature as well as with respect to temperature at a constant space velocity. The paraffin to olefin ratio increases with increasing conversion and decreases with increasing temperature. In both cases, the prediction is not as good for points at high conversions, since the model overestimates the production of olefins under these conditions. Similar changes with respect to conversion and temperature of the paraffin to olefin ratio resulting from the catalytic cracking of various hydrocarbons have been observed by others (7, 17, 45, 47, 59, 60). The ability of the model to predict experimental values at different temperatures suggests that we have used reasonable values of activation energies and preexponential factors for the rate constants.

We obtained a satisfactory fit of the experimental data for USY-S by changing the value of ΔH_+ and making minor changes in the other kinetic parameters (Table 7). The model accurately predicts that steaming causes the paraffin to olefin ratio to decrease from a value of 2.6 to a value of 1.6 at a conversion of 10–11%. These results indicate that differences in the strength of the Brønsted acid sites account for most of the changes in activity and selectivity between the two catalysts. The model also indicates that while the steam treatment decreases catalyst acidity, it does not affect the fundamental chemistry taking place on the catalytic surface.

CONCLUSIONS

We have developed a kinetic model for isobutane cracking based on carbo-cation surface chemistry. The approach is general and may be used to formulate kinetic models for the cracking of other hydrocarbons. We estimated preexponential factors by using transition state theory and data from gas phase thermodynamics, while making reasonable approximations for entropies of adsorption of gas phase carbenium ions on acid sites. We estimated activation energies by using the Evans–Polanyi correlation and gas phase thermodynamic data. We used the heat of stabilization of surface carbenium ions relative to surface protons (ΔH_+) to estimate enthalpies of reactions involving surface species. This is the only parameter that involves the catalyst surface and is related to Brønsted acid strength.

The kinetic model was effective in describing our experimental data for isobutane cracking over Y-based FCC catalysts. It accurately predicted the formation of individual gas phase species as well as changes in reaction rates and product distribution with conversion, temperature, and catalyst steaming. The key parameter that changed when modeling USY-C and USY-S was ΔH_+, indicating that USY-C had stronger Brønsted acidity. In the next paper (22), we will use information provided by our model to quantitatively analyze catalytic cycles operative during isobutane cracking and to elucidate the role of different reactions in determining catalyst activity and selectivity.

ACKNOWLEDGMENTS

We thank Stan Koziol for carrying out the kinetic measurements and Gail Hodge for the FTIR work. This work was partially supported by funds provided by Engelhard Corp. and the Office of Basic Energy Sciences of the U.S. Department of Energy (DE-FG02-84ER13183). This work was also supported in part by the U.S. Environmental Protection Agency and the Center for Clean Industrial and Treatment Technologies.

REFERENCES

1. EPA, "Clean Air Act Amendments of 1990. Detailed Summary of Titles," 1990.
2. Greensfelder, B. S., and Voge, H. H., *Ind. Eng. Chem.* **37,** 514 (1945); **37,** 983 (1945); **37** 1038 (1945); Good, G. M., Voge, H. H., and Greensfelder, B. S., *Ind. Eng. Chem.* **39,** 1032 (1947).
3. Van Hook, W. A., and Emmett, P. H., *J. Am. Chem. Soc.*, 84, 4410 (1962); **84,** 4421 (1962); Hightower, J. W., and Emmett, P. H., *J. Am. Chem. Soc.* **87,** 939 (1965).
4. Ko, A.-N., and Wojciechowski, B. W., *Prog. React. Kinet.* **12,** 201 (1983).
5. John., T. M., and Wojciechowski, B. W., *J. Catal.* **37,** 240, 348 (1975).
6. Borodzinski, A., Corma, A., and Wojciechowski, B. W., *Can. J. Chem. Eng.* **58,** 219 (1980).

7. Abbot, J., and Wojciechowski, B. W., *J. Catal.* **113,** 353 (1988).
8. Abbot, J., and Wojciechowski, B. W., *Can. J. Chem. Eng.* **66,** 817 (1988).
9. Zhao, Y., Bamwenda, G. R., Groten, W. A., and Wojciechowski, B. W., *J. Catal.* **140,** 243 (1993).
10. Liguras, D. K., and Allen, D. T., *Ind. Eng. Chem. Res.* **28**(6), 674 (1989).
11. Liguras, D. K., and Allen, D. T., *Ind. Eng. Chem. Res.* **28**(6), 665 (1989).
12. Baltanas, M. A., Raemdonck, K. K. V., Froment, G. F., and Mohedas, S. R., *Ind. Eng. Chem. Res.* **28**(7), 899 (1989).
13. Willems, P. A., and Froment, G. F., *Ind. Eng. Chem. Res.* **27**(11), 1959 (1988); Willems, P. A., and Froment, G. F., *Ind. Eng. Chem. Res.* **27**(11), 1966 (1988)
14. Lox, E. S., and Froment, G. F., *Ind. Eng. Chem. Res.* **32**(1), 71 (1993).
15. Feng, W., Vynckier, E., and Froment, G. F., *Ind. Eng. Chem. Res.* **32**(12), 2997 (1993).
16. Dumesic, J. A., Rudd, D. F., Aparicio, L. M., Rekoske, J. E., and Treviño, A. A., "The Microkinetics of Heterogeneous Catalysis." Amer. Chem. Soc., Washington, DC, 1993.
17. McVicker, G. B., Kramer, G. M., and Ziemiak, J. J., *J. Catal.* **83,** 286 (1983).
18. Lombardo, E. A., and Hall, W. K., *J. Catal.* **112,** 565 (1988).
19. Engelhardt, J., and Hall, W. K., *J. Catal.* **125,** 472 (1990).
20. Stefanadis, C., Gates, B. C., and Haag, W. O., *J. Molec. Catal.* **67,** 363 (1991).
21. Rekoske, J. E., Madon, R. J., Aparicio, L. M., and Dumesic, J. A., *in* "Proceedings, 10th International Congress on Catalysis, Budapest, July 1992" (L. Guczi, *et al.* Ed.) p. 1653. Elsevier, Amsterdam, 1993.
22. Yaluris, G., Rekoske, J. E., Aparicio, L. M., Madon, R. J., and Dumesic, J. A., *J. Catal.* **153,** 65 (1995).
23. Haden, W. L., and Dzierzanowski, F. J., U.S. Patent 3,506,594 (1970); 3,647,718 (1972).
24. Brown, S. M., Durante, V. A., Reagen, W. J., and Speronello, B. K., U.S. Patent 4,493,902 (1985).
25. Sohn, J. R., DeCanio, S. J., Lunsford, J. H., and O'Donnell, D. J., *Zeolites* **6,** 225 (1986).
26. Chen, D., Sharma, S., Cardona-Martínez, N., Dumesic, J. A., Bell, V. A., Hodge, G. D., and Madon, R. J., *J. Catal.* **136,** 392 (1992).
27. Brower, D. M., *in* "Chemistry and Chemical Engineering of Catalytic Processes" (R. Prins and G. C. A. Schuit, Eds.) p. 137, Sijthoff and Noordhoff, The Netherlands, 1980.
28. Brower, D. M., and Hogeveen, H., *Prog. Phys. Org. Chem.* **9,** 179 (1972).
29. Gates, B. C., Katzer, J. R., and Schuit, G. C., "Chemistry of Catalytic Processes." McGraw-Hill, New York, 1979.
30. Ward, J. W., *J. Catal.* **9,** 225 (1967); **10,** 34 (1968); **11,** 251 (1968).
31. Bolton, A. P., and Bujalski, R. L., *J. Catal.* **23,** 331 (1971).
32. Barthomeuf, D., and Beaumont, R., *J. Catal.* **30,** 288 (1973).
33. Haag, W. O., Lago, R. M., and Weisz, P. B., *Nature* **309,** 589 (1984).
34. Hopkins, P. D., *J. Catal.* **12,** 325 (1968).
35. Lunsford, J. H., *J. Phys. Chem.* **72,** 4163 (1968).
36. Beyerlein, R. A., McVicker, G. B., Yacullo, L. N., and Ziemiak, J. J., *J. Phys. Chem.* **92,** 1967 (1988).
37. Jacobs, P. A., Leeman, H. E., and Uytterhoeven, J. B., *J. Catal.* **33,** 17 (1974).
38. Mirodatos, C., and Barthomeuf, D., *J. Chem. Soc. Chem. Commun.*, 39 (1981).
39. Haag, W. O., and Dessau, R. M., *in* "Proceedings, 8th International Congress on Catalysis, Berlin, 1984," Vol. 2, p. 305.
40. Hattori, H., Takahashi, O., Takagi, M., and Tanabe, K., *J. Catal.* **68,** 132 (1981).
41. Chen, F. R., and Fripiat, J. J., *J. Phys. Chem.* **96,** 819 (1992).
42. Brower, D. M., *Recl. Trav. Chim.* **87,** 1435 (1968).
43. Hilaireau, P., Bearez, C., Chevalier, F., Perot, G., and Guisnet, M., *Zeolites* **2,** 69 (1982).
44. Shertukde, P. V., Marcelin, G., Sill, G. A., and Hall, W. K., *J. Catal.* **136,** 446 (1992).
45. Shigeishi, R., Garforth, A., Harris, I., and Dwyer, J., *J. Catal.* **130,** 423 (1991).
46. Wielers, A. F. H., Vaarkamp, M., and Post, M. F. M., *J. Catal.* **127,** 51 (1991).
47. Corma, A., Miguel, P. J., and Orchilles, A. V., *J. Catal.* **145,** 171 (1994).
48. Stamires, D. N., and Turkevich, J., *J. Am. Chem. Soc.* **86,** 749 (1964).
49. Turkevich, J., Nozaki, F., and Stamires, D. N., *in* "Proceedings, 3rd International Congress on Catalysis, Amsterdam, 1964," p. 586.
50. Benson, S. W., "Thermochemical Kinetics." Wiley, New York, 1976.
51. Dean, J. A., "Lange's Handbook of Chemistry." McGraw-Hill, New York, 1979.
52. Stull, D. R., Westrum, E. F., Jr., and Sinke, G. C., "The Chemical Thermodynamics of Organic Compounds." Wiley, New York, 1969.
53. Aue, D. H., and Bowers, M. T. *in* "Gas Phase Ion Chemistry, (M. T. Bowers, Ed.), Vol. 2, p. 1. Academic Press, New York, 1979.
54. Stull, D. R., and Prophet, H., "JANAF Thermochemical Tables." NSRDS-NBS 37, Washington, DC, 1971.
55. Thinh, T. P., Duran, J. L., Ramalho, R. S., and Kaliaguine, S., *Hydrocarbon Process.* **Jan.** 98 (1971).
56. Laidler, K. J., "Chemical Kinetics." Harper & Row, New York, 1987.
57. Sharma, S. B., Meyers, B. L., Chen, D. T., Miller, J., and Dumesic, J. A., *Appl. Catal.* **102,** 253 (1993).
58. Dumesic, J. A., Milligan, B. A., Greppi, L. A., Balse, V. R., Sarnowski, K. T., Beall, C. E., Kataoka, T., and Rudd, D. F., *Ind. Eng. Chem. Res.* **26,** 1399 (1987).
59. Corma, A., and Orchillés, A. V., *J. Catal.* **115,** 551 (1989).
60. Kogelbauer, A., and Lercher, J. A., *J. Catal.* **125,** 197 (1990).